JGR Oceans

RESEARCH ARTICLE

10.1029/2025JC023952

Ice-Sheet–Ocean Interactions and the Reversibility of a Regime Shift Beneath Filchner-Ronne Ice Shelf

Ronja Reese[1], **Jan De Rydt**[1], **and Kaitlin A. Naughten**[2]

[1]School of Geography and Natural Sciences, Northumbria University, Newcastle, UK, [2]British Antarctic Survey, Cambridge, UK

Abstract Future atmospheric warming could cause an abrupt increase in ocean temperature beneath the Filchner–Ronne Ice Shelf, Antarctica, from −2.2°C to more than 0°C in a few decades. In simulations, such a transition leads to a twenty-fold increase in sub-shelf melt rates, driving a retreat of the ice sheet. Here we investigate the evolution and reversibility of the ocean and ice sheet states using coupled ice-sheet–ocean model simulations. We show that sub-shelf melt rates increase only half as much as in the uncoupled system, and we find that, after a period of climate cooling, the cavity is reversible from warm to cold conditions, independently of ice-ocean interactions related to regional changes in sub-shelf melting, cavity geometry, and ocean dynamics. In contrast to the abrupt warming transition, the recovery of a cold ocean state takes more than a century. Meanwhile the ice sheet continues to lose mass and contribute to sea level rise with a maximum rate of up to 0.9 mm/a.

Plain Language Summary Floating ice shelves fringe most of the Antarctic continent. The second largest ice shelf, the Filchner–Ronne ice shelf is located in the southern Weddell Sea. The ocean water in the cavity underneath the ice shelf is currently cold and ocean-driven melting is low. However, climate change could, in extreme scenarios, cause a sudden inflow of warm water into the cavity, which would drive a factor 20 increase in melting, and subsequent ice loss from the Antarctic continent. Here, we use numerical models to analyze how the ice sheet and ocean evolve together, allowing for feedbacks and interactions between both to occur. We find that sub-shelf melt rates increase only half as much as when interactions are not fully accounted for. Moreover, we find that the ocean can reverse back to a cold state if atmospheric conditions are reversed. However, this transition takes more than a century, and meanwhile the ice sheet continues to lose mass and contribute to sea level rise. The maximum rate of ice loss we find in the Weddell Sea sector is about a factor 3 larger than the current ice loss estimate for the entire continent.

Key Points:

- A shift to warm ocean conditions below the cold Filchner–Ronne Ice Shelf induces high rates of ice loss up to 0.9 mm/a sea level equivalent
- Melt rates under warm ocean cavity conditions are 50% lower in coupled ice-sheet–ocean simulations compared to those with a static cavity
- When ramping down the climate forcing, the cavity regains—delayed by a century—a cold state despite changes in geometry and melt

Supporting Information:

Supporting Information may be found in the online version of this article.

Correspondence to:

R. Reese,
ronja.reese@northumbria.ac.uk

Citation:

Reese, R., De Rydt, J., & Naughten, K. A. (2026). Ice-sheet–ocean interactions and the reversibility of a regime shift beneath Filchner-Ronne ice shelf. *Journal of Geophysical Research: Oceans*, *131*, e2025JC023952. https://doi.org/10.1029/2025JC023952

Received 23 DEC 2025
Accepted 15 APR 2026

Author Contributions:

Conceptualization: Ronja Reese, Jan De Rydt, Kaitlin A. Naughten
Data curation: Ronja Reese, Kaitlin A. Naughten
Formal analysis: Ronja Reese
Investigation: Ronja Reese
Methodology: Ronja Reese, Jan De Rydt, Kaitlin A. Naughten
Software: Ronja Reese, Jan De Rydt, Kaitlin A. Naughten
Validation: Ronja Reese
Visualization: Ronja Reese
Writing – original draft: Ronja Reese
Writing – review & editing: Ronja Reese, Jan De Rydt, Kaitlin A. Naughten

1. Introduction

At present, melting at the base of the Filchner–Ronne Ice Shelf in Antarctica (FRIS, Figure 1) is primarily driven by High Salinity Shelf Water (HSSW), which is a cold and saline water mass that forms in austral autumn and winter as a result of sea ice production in the Southern Weddell Sea (Haid & Timmermann, 2013). Because HSSW forms at the surface, its temperature is around −2.2°C, which is close to the surface freezing point and, due to the pressure-dependency, 1°C above the local freezing point when in contact with the deepest parts of the ice shelf. This results in relatively low sub-shelf melt rates on the order of 1 m/a (Vaňková & Nicholls, 2022; Zeising et al., 2022). As HSSW is the densest water mass on the continental shelf, it prevents warmer waters that reside offshore of the continental shelf break from coming into contact with the ice sheet (Janout et al., 2021).

Under future atmospheric warming, however, the continental shelf is expected to freshen: for some of the most extreme greenhouse gas emission scenarios, such as SSP5-8.5 (Mathiot & Jourdain, 2023), A1B (Haid et al., 2023; Hellmer et al., 2012) and idealized 1%CO2 and abrupt-4xCO2 scenarios (Naughten et al., 2021), the density gradient across the continental slope front eventually weakens enough to enable the intrusion of Warm Deep Water (WDW) onto the continental shelf, predominantly through the Filchner Trough (Figure 1). This regime shift from a "cold" to a "warm" ocean state happens within one decade (Haid & Timmermann, 2013) to three decades (Hellmer et al., 2012, 2017), and as early as the end of the 21st century (Hellmer et al., 2012).

Once WDW enters the FRIS cavity, melt rates increase by a factor of twenty (Hellmer et al., 2012; Naughten et al., 2021), causing pervasive ice-shelf thinning, a loss of buttressing forces, and the speed-up of ice that flows across the grounding line, see Figure 1. Estimates from ice-sheet simulations indicate that the new melt-rate

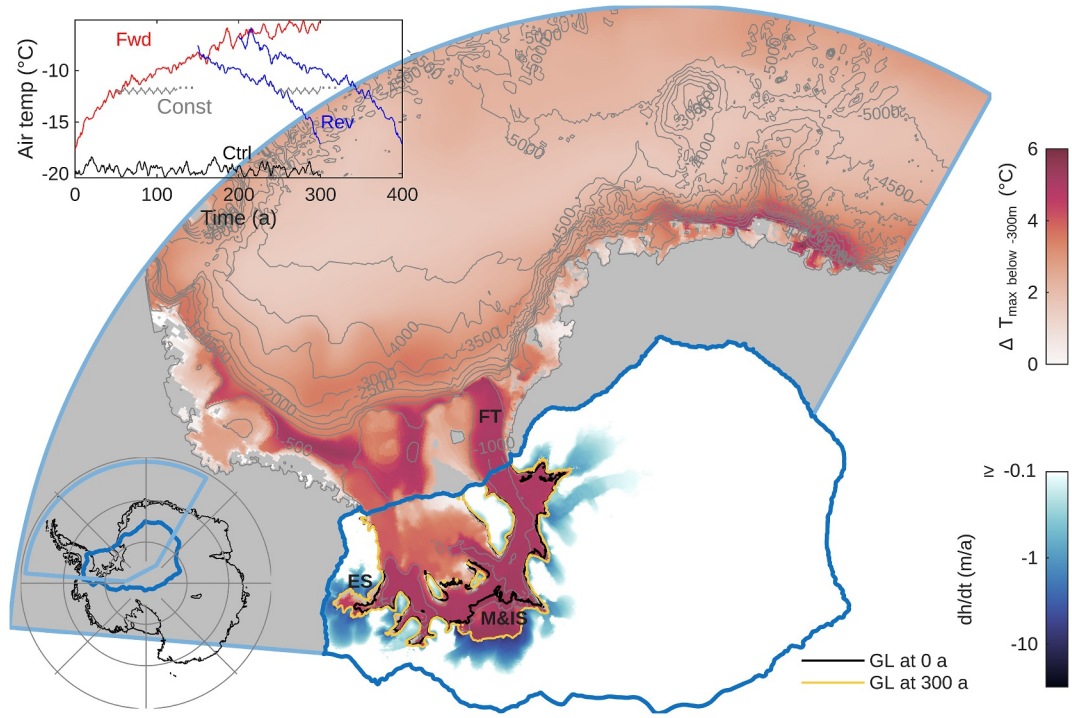

Figure 1. Coupled ocean and ice sheet response to 300 years of extreme climate forcing in the Weddell Sea. Red colors indicate the difference in maximum ocean temperatures below −300 m between present-day and after 300 years of abrupt-4xCO2 forcing (Fwd-IO, see Section 2.2 and Table S1 in Supporting Information S1). In areas that unground during the coupled simulation, we use the in situ freezing point at the depth of the bathymetry as baseline temperature. Labeled gray contours show the bathymetry. Grounding lines retreat from their present-day position (black) to the position indicated in yellow. Corresponding rates of ice thickness change (dh/dt) of the grounded ice sheet at the end of the 300-year simulation are shown in blue. Blue lines outline ice sheet (dark) and ocean (light) modeling domains. The lower inset indicates their location in Antarctica. FT stands for Filchner Trough, ES for Evans Ice Stream, M&IS for Moeller and Institute ice streams. Upper left inset exemplifies experimental design of this study by showing the spatially averaged air temperature evolution over the Southern Weddell Sea continental shelf in the Ctrl, Fwd, and Rev experiments detailed in Section 2.2.

regime causes ice loss between 1 and 10 cm sea-level equivalent, over 100 years (Hill et al., 2024). These simulations are based on parameterized sub-shelf melt rates, and do not capture the complex interactions between ocean dynamics, melt rates and changes in ice-sheet geometry. Simulations by Naughten et al. (2021) included a dynamically active ice sheet, but since the transition from a cold to a warm ocean state only occurred in the final decades of the simulations, the longer-term response of the ice sheet to WDW exposure was not explored.

The coupled ice-sheet–ocean system, in which both melt rates and the ice sheet respond and feed back onto the ocean circulation, is expected to evolve differently in comparison to its individual, uncoupled parts for a number of reasons. Changes in the geometry of the ice-shelf cavity can enhance or reduce melting through changes in cavity circulation, adjustments of the local freezing point at the ice-shelf base, and modulation of the water masses adjacent to the shelf base (De Rydt & Naughten, 2024; Holland et al., 2023). Spatial and temporal changes in freshwater fluxes from melting can affect ocean circulation and stratification and thereby influence basal melt rates (Jourdain et al., 2017). Differences in basal melt rates then, in the coupled system, feed back to the ice sheet, thereby influencing its dynamic response. For example, Timmermann and Goeller (2017) found slightly higher melt rates in a coupled simulation compared to a fixed geometry, with a detailed analysis of the ice sheet response remaining open.

Besides understanding the centennial evolution of the Filchner–Ronne Ice Shelf after a transition to a warm state in a coupled configuration, another open question is whether the cavity exhibits bi-stability for current climate conditions. Bi-stability means that the system has two distinct equilibrium states for the same external climate conditions, and which state is attained depends on its history, see for example, Strogatz (2018). Simulations of Hellmer et al. (2017) indicated bi-stability: after a transition to a warm cavity state, incursions of WDW onto the

continental shelf are sustained, even when atmospheric conditions and sea ice concentrations were reversed to modern-day values.

Hellmer et al. (2017) report that bi-stability of the system was due to a positive meltwater feedback, whereby increased melting after the warm transition enhances the density-driven onshore transport of heat, driving further melting, and thereby sustaining the warm state. Bi-stability was also found by Hazel and Stewart (2020) who demonstrated that for an initial fresh perturbation to the hydrography of the FRIS cavity, the ocean evolves to a warm state, whereas for an unchanged present-day hydrography, the cavity remains cold. Bi-stability is also apparent in other numerical setups and for different climate forcings, see for example, Haid et al. (2023), but its existence depends on the details of the experiments. All studies that investigated reversibility have been conducted for a static, present-day ice-shelf geometry.

The primary aim of this work is to quantify the importance of ice-ocean interactions and feedbacks for the multi-centennial response of the coupled FRIS-Weddell Sea system. We analyze the ice sheet response to a regime shift of the ocean state within the FRIS cavity, the response of the ocean state to changes in ice-shelf geometry and concurrent changes in basal melt rate, and the existence of bi-stability in the coupled system. To this aim, we extend the regional, coupled ice-sheet and ocean simulations from Naughten et al. (2021). We test for reversibility and bi-stability by forcing the model with reverse and constant atmospheric conditions, respectively. To quantify the role of feedbacks and interactions between ice and ocean dynamics, we compare the results to simulations with a fixed, present-day cavity geometry.

2. Methods and Experimental Design

2.1. Ice-Sheet–Ocean Coupled Modeling Setup

All simulations in this study are performed with the coupled ice-sheet–ocean model Úa-MITgcm, which was developed by De Rydt and Gudmundsson (2016) for simplified geometries and boundary forcing, and adapted for realistic domains by Naughten et al. (2021) and De Rydt and Naughten (2024). A detailed description of the configuration used here is presented in Naughten et al. (2021). We summarize its key components. The offline exchange of basal melt rates and ice-shelf draft between the ocean model MITgcm (Losch, 2008; Marshall et al., 1997) and the ice sheet model Úa (Gudmundsson, 2013) occurs at fixed time intervals, chosen to be 1 year. At each coupling step, key quantities, such as the ocean hydrography, currents and sea ice properties are preserved. Ocean cells can close or open to accommodate changes in the cavity geometry, and hydrographic properties of newly wetted cells are extrapolated from neighboring cells.

The extent of the regional ocean and ice-sheet domains is shown in Figure 1. At the lateral ocean boundaries and at the ocean surface, boundary conditions from the United Kingdom Earth System Model were applied (UKESM1-0-LL from CMIP6; Sellar et al., 2019). A rotation and scaling correction was applied to the coastal winds, as described in Naughten et al. (2021), whereas biases in other UKESM fields were found to be small. No restoring of salinity or temperatures was used. Simulations with historical forcing from UKESM were shown to produce basal melt rates and ocean hydrographic properties in good agreement with observations (Naughten et al., 2021). Surface accumulation rates in the ice sheet model were set to a constant present-day climatology (Lenaerts et al., 2012) and the ice front was kept fixed, that is, calving was assumed to occur at the rate required to maintain the current location of the ice front. While we do not keep track of changing calving flux to the ocean, we apply a constant climatological freshwater flux to represent iceberg melt in the correct spatial pattern. Note that ice shelves contained in the ocean domain, excluding FRIS, are static, but have changing freshwater fluxes over time which can impact the FRIS water mass properties, for example, as meltwater travels downstream on the coastal current. The initial state of the coupled model was obtained through a series of inverse (Úa) and spin-up (Úa and MITgcm) simulations, resulting in a present-day representation of the Southern Weddell Sea and its adjacent ice-sheet basins (Naughten et al., 2021).

2.2. Experimental Design

We performed three different types of simulations: forward (*Fwd*) experiments forced by abrupt-4xCO2 climate data from UKESM, reverse (*Rev*) experiments with the same climate forcing but reverted in time, and constant (*Const*) experiments where the forcing is fixed to a specific climatic state. Experiments are carried out with the coupled ice-sheet–ocean model (Fwd-IO, Rev-IO, Const-IO), and some also with the stand-alone ocean model

using a static present-day cavity (Fwd-O, Rev-O). To provide a benchmark, we perform control simulations (Ctrl-IO and Ctrl-O) forced by a cyclic repetition of UKESM historic control forcing. All experiments are summarized in Table S1 in Supporting Information S1 and exemplified in the inset in Figure 1. Further details are as follows.

For the Fwd-IO experiments, we extended the 150-year long abrupt-4xCO2 simulations from Naughten et al. (2021) by 150 years. The 300-year long timeseries of boundary conditions was obtained from a recently extended simulation of UKESM (Met Office Hadley Centre, 2026). Figures S1 and S2 in Supporting Information S1 show the evolution of atmospheric temperatures and winds during the 300 years, respectively. In agreement with Naughten et al. (2021), regular incursions of WDW onto the eastern continental shelf start to occur after approximately 75 years, followed by flooding of the entire shelf around year 150. We repeated the 300-year experiment for a fixed present-day ice-shelf geometry (Fwd-O).

Zero and 50 years after the full transition to warm shelf conditions (150 and 200 years into the Fwd-IO simulation, respectively), we reversed the atmospheric forcing and open ocean boundary conditions (experiments Rev-IO-150 and Rev-IO-200). Rather than applying a step-change in the forcing, the time dimension was mirrored, such that changes occur at the same rate as in the Fwd simulations, but in the opposite direction (e.g., cooling instead of warming; note that within each year the monthly order remained unchanged). This allowed us to test for reversibility without introducing a potential (numerical) shock to the system that can dominate the response. Reverse experiments were repeated with a stand-alone ocean model (Rev-O-150 and Rev-O-200).

To test for bi-stability, we branched the Fwd and Rev simulations after years 25, 55 and 75, whilst keeping the climate forcing constant (Const-IO-25, Const-IO-55, Const-IO-75, and ConstR-IO-25, ConstR-IO-55 ConstR-IO-75). To reduce biases, we retained some natural variability in the forcing by cycling through one decade of atmospheric and open ocean boundary conditions. For example, experiments Const-IO-25 and ConstR-IO-25 were cyclically forced by boundary conditions between year 20 and year 29. Finally, we perform fixed cavity experiments with higher and lower melt rates by adjusting the drag coefficient in the boundary layer parameterization by multiplying and dividing by a factor of 4 (Fwd-O-high, Fwd-O-low, Rev-O-150-high, and Rev-O-150-low).

3. Results and Discussion

3.1. High Rates of Ice Loss

The incursion of WDW into the Filchner-Ronne cavity, as simulated in the Fwd-IO experiment, causes substantial thinning of the ice shelf, grounding line retreat and upstream ice loss between year 150, when the grounding line is exposed to WDW, and year 300 (Figures 1 and 2). Extensive retreat occurs in the marine basin that is drained by the Moeller and Institute ice streams, where ice-sheet thinning rates exceed 10 m/a, consistent with Hill et al. (2024). We additionally simulate a 100 km retreat of the Evans Ice Stream, which, over long timescales, could link to marine basins in West Antarctica (Morlighem et al., 2020; Pritchard et al., 2025; Vaughan et al., 2011). The total loss of ice within the domain, following about 150 years of ice-shelf exposure to WDW, is 10 cm sea-level equivalent, with a maximum rate of 0.9 mm/a, see Figures 2b and 2c.

Once exposure to WDW pushes the ice sheet into a state of negative mass balance, recovery of its modern-day state might not be possible, or could take millennial time scales, even if cold ocean conditions were reestablished (Hill et al., 2024; Reese et al., 2023). The response of the ice sheet in a cooling scenario is analyzed in the Rev-IO experiments, which are branched off from the Fwd-IO experiment with atmospheric fields that are gradually ramped down to present-day conditions, see Section 2.2. In the Rev-IO-150 scenario where atmospheric temperatures peak at the onset of ice-sheet exposure to WDW, that is, after 150 years into the Fwd-IO experiment, the ice-sheet still experiences pervasive grounding line retreat (Rev-IO-150 in Figure 2a). Figure 2c shows that ice loss rates reach 0.5 mm/a sea level equivalent, about 100 years after the peak in atmospheric temperatures. This delay can be understood as follows. During the gradual reversal to cooler and drier atmospheric conditions, WDW continues to intrude into the cavity. Colder ocean conditions are only gradually re-established over a period of about 150 years (see Section 3.3 for an analysis of the ocean state), during which the ice-shelf melt rates remain elevated above present-day values, as depicted by the blue curve in Figure 3a. Higher melt rates, in combinations with internal, possibly self-sustaining ice dynamics, continue to drive ice-sheet mass loss well beyond the onset of atmospheric cooling. The Rev-IO-200 experiment shows a similar behavior, see Figure S4 in Supporting Information S1, with a 20-year delay between maximum global temperatures and maximum rates of ice loss. Since

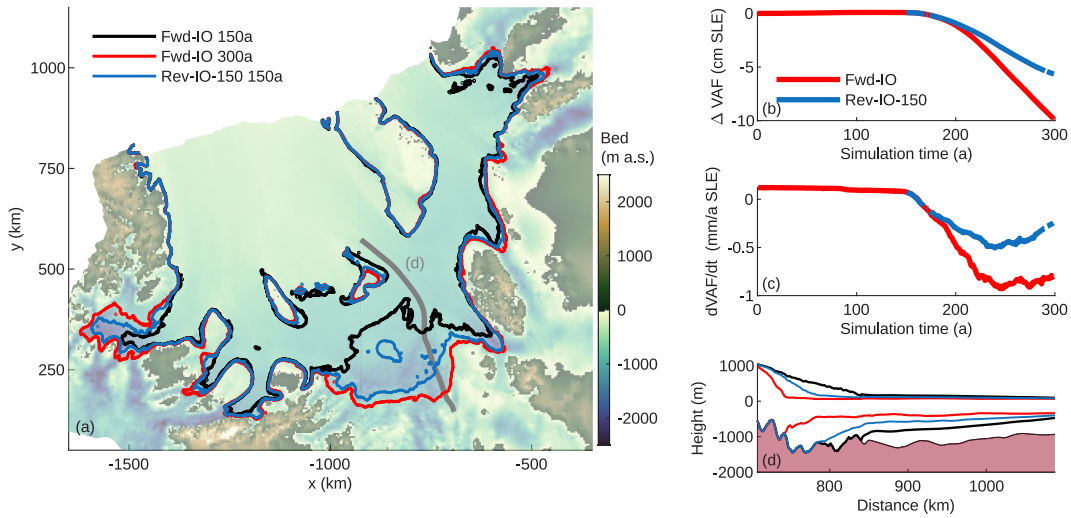

Figure 2. Ice-sheet response to a cold-to-warm and subsequent warm-to-cold transition of the Weddell Sea continental shelf. (a) Regional bedrock with grounding line positions after 150 and 300 years in the cold-to-warm simulation (Fwd-IO) and after 150 years into the reverse simulation (warm-to-cold, Rev-IO-150) which starts at year 150 of Fwd-IO. The gray dashed line indicates the location of the flowline in panel (d). (b) Evolution of the ice volume above floatation (SLE is Sea Level Equivalent) in the forward and reverse simulations, relative to the control simulation (Ctrl-IO). (c) Evolution of the rates of ice loss for the forward and reversal simulations. (d) Lateral view of the ice sheet geometry along a flowline for the times depicted in panel (a).

climate conditions in this reverse simulation peak later and at more extreme levels, the maximum rate of ice loss is close to that in the forward Fwd-IO simulation.

In all forward and reverse experiments in which WDW accesses the FRIS cavity, the grounded ice continues to thin by the end of the simulations, and the ice sheet does not generally reach an equilibrium within the simulated timescales. Testing reversibility of the ice sheet typically requires millennial timescales (Hill et al., 2024; Reese et al., 2023), and we cannot make statements about instability-driven retreat of the ice sheet from our experiments.

3.2. Melt Rates Diverge Between an Evolving and a Fixed Cavity Geometry

Before the transition from its currently cold to a warm cavity state (years 0–150 in the Fwd-IO experiment), the FRIS cavity geometry remains largely unchanged, and changes in ocean dynamics are driven by changes in the atmosphere and the ocean boundary. However, once WDW floods the cavity, two-way interactions between ocean and ice-sheet dynamics will influence the evolution of the coupled system. To quantify the importance of these interactions for the ocean dynamics, we compare results from the coupled simulations (Fwd-IO) to simulations with a static, present-day cavity geometry (Fwd-O). During the regime shift, melt rates initially increase by a similar amount in both experiments, see Figure 3a. However, from year 170, melt rates start to diverge, as the cavity geometry adjusts in response to the elevated melt rates. While in the fixed cavity run, melt rates continue to increase, melt rates in the coupled simulation plateau at around 1,700 Gt/a and subsequently decrease slightly. The difference in melt rates at the end of both simulations is a factor of two.

In the coupled simulations, the slope of the ice draft steepens in regions near the grounding line (Figure 2d), where melt rates increase from a few meters per year in the beginning to over 50 m/a at the end of the simulation (Figure 4). The highest melt rates track the grounding line as it retreats. Further downstream, the ice shelf thins to a shallow sheet with uniform thickness of around 400 m, where melt rates do not exceed 5 m/a. The changes in melt rate are dominated by an increase in thermal driving at the ice base, defined as the temperature difference between the ambient ocean and the local freezing point. This change is most prominent near the grounding line, see Figure 4. Changes in the mixed layer speed, or equivalently, changes in turbulent mixing of heat toward the ice base, are confined to distinctive outflow pathways, most noticeably along western and eastern boundaries (Figure 4). In contrast to our finding of lower melt rates in the coupled case, Timmermann and Goeller (2017) report a slight increase in melt fluxes. Differences likely arise due to less simulated ice-shelf thinning and grounding line retreat in their configuration, see Figure 9 in Timmermann and Goeller (2017).

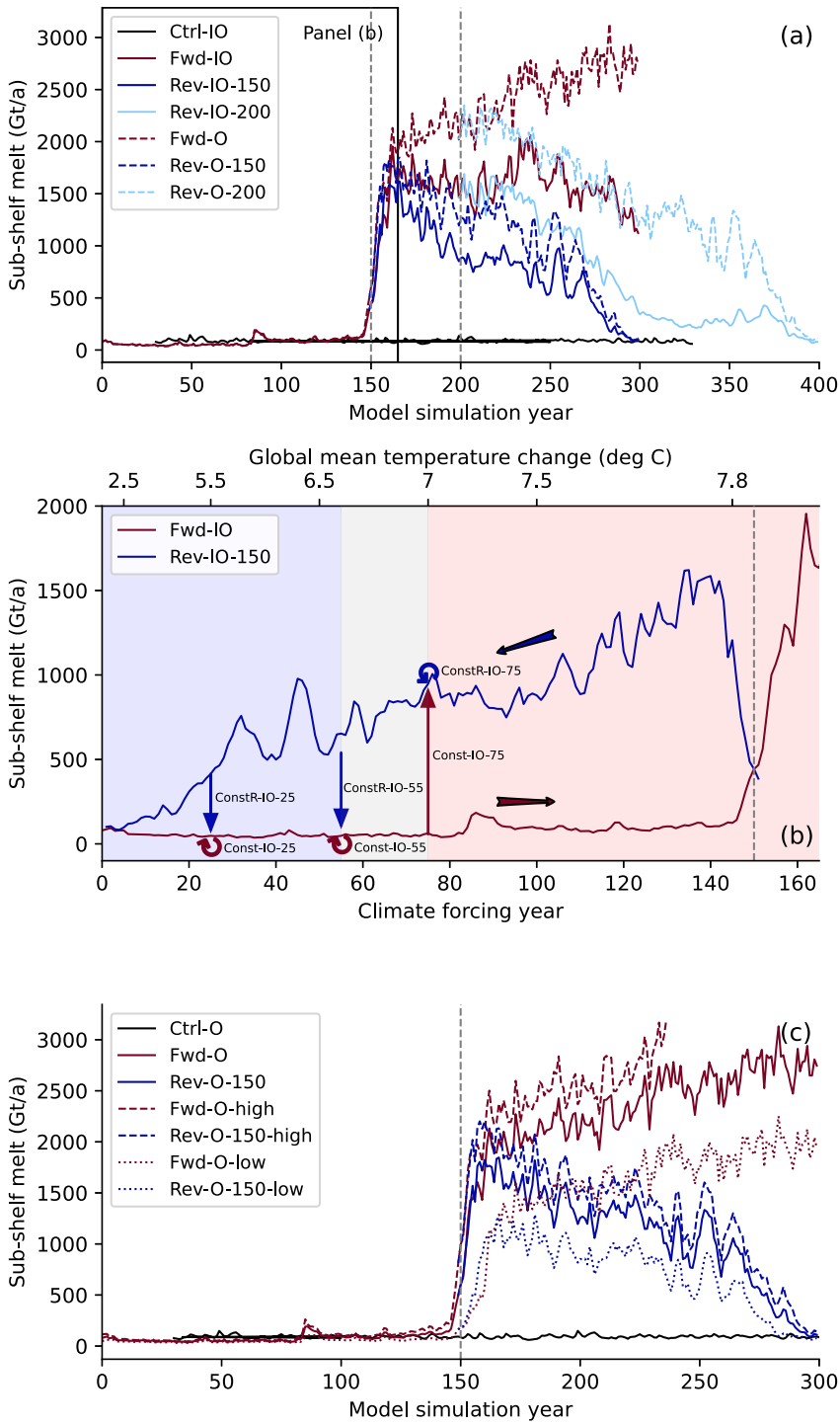

Figure 3. Sub-shelf melt rate evolution, reversibility of the ocean state and the impact of ice-ocean feedbacks. (a) Evolution of sub-shelf melt rates for a dynamically evolving ice sheet (Ctrl-IO, Fwd-IO and Rev-IO) and a fixed present-day geometry of the ice shelf (Fwd-O and Rev-O). The forward simulations are forced by abrupt-4xCO2 conditions, the reverse simulations branch off from the forward experiments after 150 and 200 years. Solid black box indicates extent of panel (b). Gray dashed vertical lines show timing when reverse runs are branched off. (b) Annual mean sub-shelf melt rates for the forward (in red, Fwd-IO) and reverse (in blue, Rev-IO-150) simulations, with the time direction indicated by the horizontal red and blue arrows, respectively. The corresponding global mean temperature changes are shown at the top. Constant climate simulations (Const-IO) are started from the forward and reverse experiments and repeatedly cycled through the climate forcing of the corresponding decade. Vertical red and blue arrows indicate Const-IO runs that transition from a cold (red) to a warm (blue) cavity state, respectively. Blue (red) shading indicates climate conditions with a cold (warm) steady cavity state. (c) Evolution of sub-shelf melt rates over time in forward and reverse simulations for the fixed cavity with higher and lower melting.

Conversely, when the geometry of the ice shelf is not evolved in time (Fwd-O in Figure 4), a widespread increase in mixed layer velocity is simulated. This increase is sustained by the overall steeper slopes, and together with the enhanced thermal driving near the grounding line, leads to an amplification of the melt rates over a much larger portion of the ice shelf. Melt rates are further amplified by high thermal driving in downstream regions where the shelf base remain exposed to deep, warm water masses, such as in the Filchner Ice Shelf. This explains the factor of two difference in total melt volume compared to the coupled simulations (Figure 3a).

3.3. Asymmetric Reversibility of the Ocean State

As noted in Section 3.1, the reversal of the atmospheric forcing in the Rev-IO-150 experiment is sufficient to revert to cavity temperatures and meltwater volumes that are near-identical to present-day values, see Figure 3a. The same applies when atmospheric conditions are reverted later, as illustrated by the Rev-IO-200 experiment. The main difference between the Rev-IO-150 and Rev-IO-200 experiments is a significant change in the cavity geometry, which does not play a role in the reversibility of the system.

In contrast to the Fwd-IO experiments, the change in melt rates indicating a transition from a warm to a cold cavity state does not occur abruptly, that is, within less than two decades, but rather unfolds over a centennial timescale, see Figure 3b. The different ocean states for the same climate conditions in the forward and reverse runs could hint at bi-stability, that is, that two distinct stable states of the ice-ocean system exist. Bi-stability refers to an equilibrium state and can be analyzed by branching Fwd-IO and Rev-IO simulations at a given time, and keeping the climate forcing constant. We tested branching at $t_b = 25$, 55 and 75 years in the Fwd-IO simulation, and at the equivalent climate forcing in the Rev-IO-150 simulation, see Section 2.2. For climate conditions around $t_b = 55$ years starting from a cold state (Const-IO-55) the cavity remains cold, and branching off from an intermediate warm state (ConstR-IO-55), the ocean equally evolves to a cold state, see Figure 3b and Figure S5 in Supporting Information S1. The same holds true for the Const-IO-25 and ConstR-IO-25 experiments, and indicates that for atmospheric conditions with a global mean temperature change in UKESM at or below 6.6°, the FRIS cavity remains in its cold state. For climate conditions around $t_b = 75$ years the ocean transitions to a warm state (Const-IO-75), even though at $t_b = 75$ no regular intrusions of WDW into the cavity were simulated in the transient Fwd-IO experiment. Starting from the corresponding intermediate warm state (ConstR-IO-75), the cavity remains warm. Hence, for global mean temperature changes in UKESM at or above 7°, the FRIS cavity transitions to a warm state.

To understand the apparent asymmetry between the abrupt cold-to-warm and the more gradual warm-to-cold transition, we diagnose the evolution of water masses on the continental shelf. In the Fwd-IO experiment, Naughten et al. (2021) identified two stages leading to the major cavity transition. In stage 1, which lasts until year 79, melt rates decrease and the cavity circulation weakens, due to a gradual and continuous freshening of the continental shelf and cavity, see Figures 5 and 6. They linked the freshening to a local increase in sea-ice melting, advection of fresher water masses into the domain, and—at a later stage of the simulation—reduced sea-ice formation, see also Figure 7b. In stage 2, which beings around year 80, WDW intrudes repeatedly onto the continental shelf and into the cavity, which leads to a gradual warming in the deep cavity, see Figures 6a and 6b, and melting increases slightly. Note that consistently this is around the same atmospheric forcing level at which we find that if climate conditions remained at this level a cold-to-warm transition still occurs, as demonstrated in the Const-IO-75 in Figure S5 in Supporting Information S1. The major shift to a warm cavity between years 145 and 165 is linked to a reversal of the flow through the Filchner Trough (Naughten et al., 2021), from a net outflow of cold shelf water to an inflow of warm WDW, see Figure 7d. This shift propagates from the Filchner to the Ronne Ice Shelf, with a few years offset between the intrusion of WDW indicated by the sudden warming and harmonization of water mass densities in different locations in the Filchner and Ronne ice shelves, see Figure 6. The full flushing of the cavity fully unfolds during the initial years of the Rev-IO-150 simulations. In the outer Ronne cavity and on the Ronne shelf, salinity drops before warming occurs, which could be ice shelf meltwater from the Filchner being pushed into the Ronne, and reaching the cavity slightly earlier than the WDW.

After the transition to a warm cavity, there is a strong stratification on the continental shelf between the dense, warm WDW underlying a layer of fresher, cold surface waters, see transects through Ronne and Filchner in Movies S1–S4. This is indicated also by the fact that surface waters are no longer mixed through the entire water column on the continental shelf, see Figure 7c. The lighter, cold waters overlying the WDW on the continental

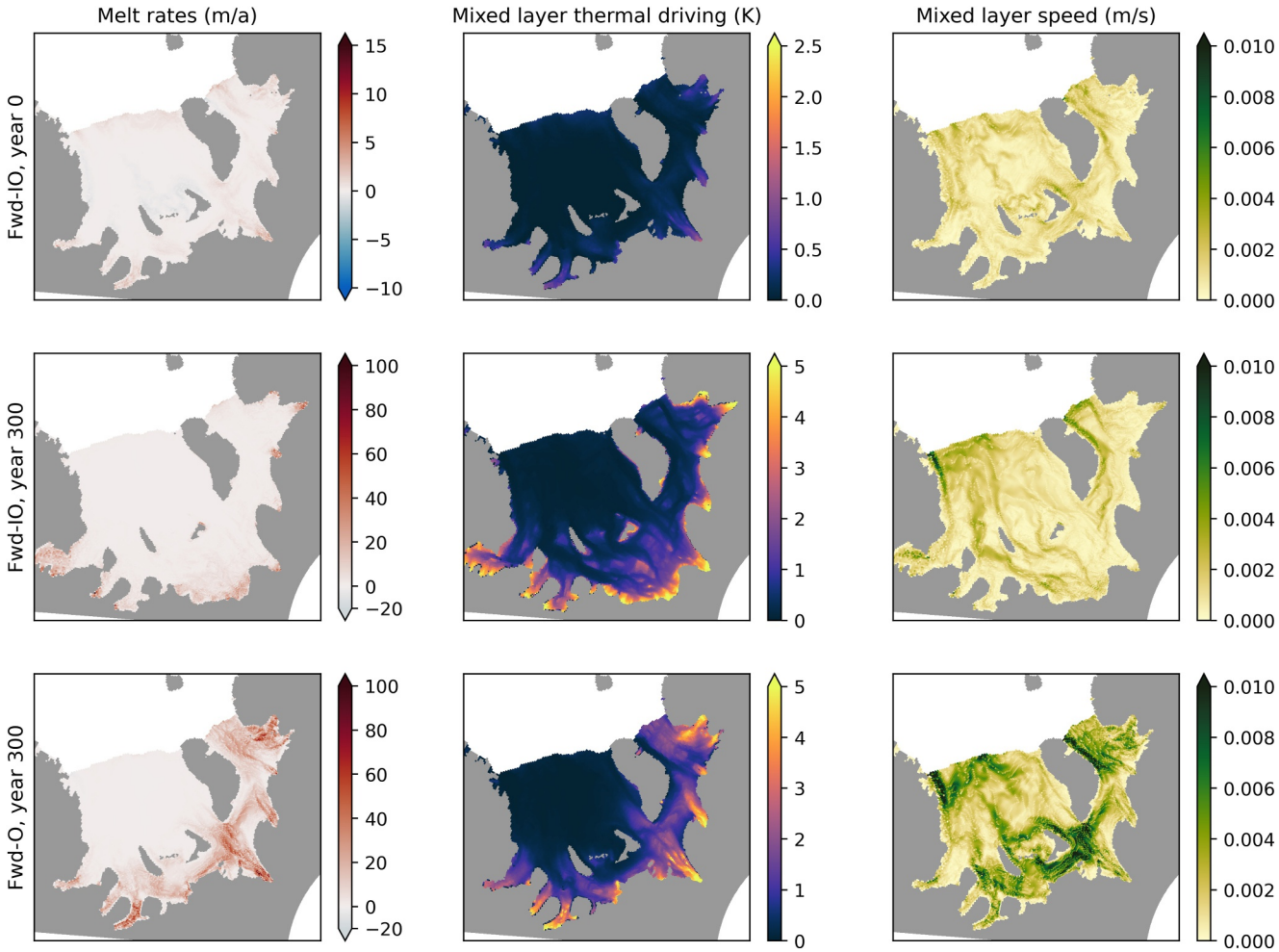

Figure 4. Melt rates and mixed layer properties underneath the ice shelf. Shown are sub-shelf melt rates, mixed layer thermal driving and mixed layer speed of the initial state and the final state in the coupled and non-coupled abrupt-4xCO2 runs (Fwd-IO, Fwd-O). Mixed layer thermal driving is calculated as $T - T_f$ where T is in situ temperature for the uppermost ocean cell adjacent to the ice base and T_f is the local in situ freezing point. Note the different scales in the upper panels.

shelf can be seen in the "wiggles" of lower density along the transect through Filchner trough in the later stages of the forward and the reverse simulation, see Figure 5b.

When climate conditions are reverted (Rev-IO-150 experiment), the gradual reversal in ice-shelf melt is not reflected in all ocean diagnostics. Initially, the difference in sub-shelf melt rates between Fwd-IO and Rev-IO appears to be caused by two factors: (a) a trend in WDW temperatures offshore (potentially due to the reversal of the ocean boundary conditions, and the reversal of a shoaling of the thermocline in the forward simulations, see Figure S3 in Supporting Information S1), as indicated by the temperatures in the cavity tracing those from offshore water masses, see Figures 6a and 6b, and (b) a gradual reduction in the southwards transport of WDW through Filchner trough, see Figure 7d. After year 75 following the reversal, the Ronne continental shelf and outer cavity densities gradually increase, see Figure 6e, as sea ice production increases, see Figures 7a and 7b, and mixing of waters masses cooled at the surface starts reaching deeper layers, see Figure 7c. In contrast to the sea-ice production and area, which are controlled by atmospheric conditions, the mixed layer depth shows an asymmetry between the Fwd and Rev simulations due to the absence—in the forward—or presence—in the reverse run—of WDW on the continental shelf that is denser than the surface water. Once densities of the Ronne continental shelf water masses increase to the density of the WDW present in the deeper cavity, the cold water masses replace the WDW abruptly, see Figure 6. This starts in the deeper Ronne cavity, and propagates with a time lag of a few years into the deep Filchner, outer Filchner cavity and then on the Filchner continental shelf close to the end of the reverse simulation. Circulation through Filchner trough reverts to its initial net outflow as

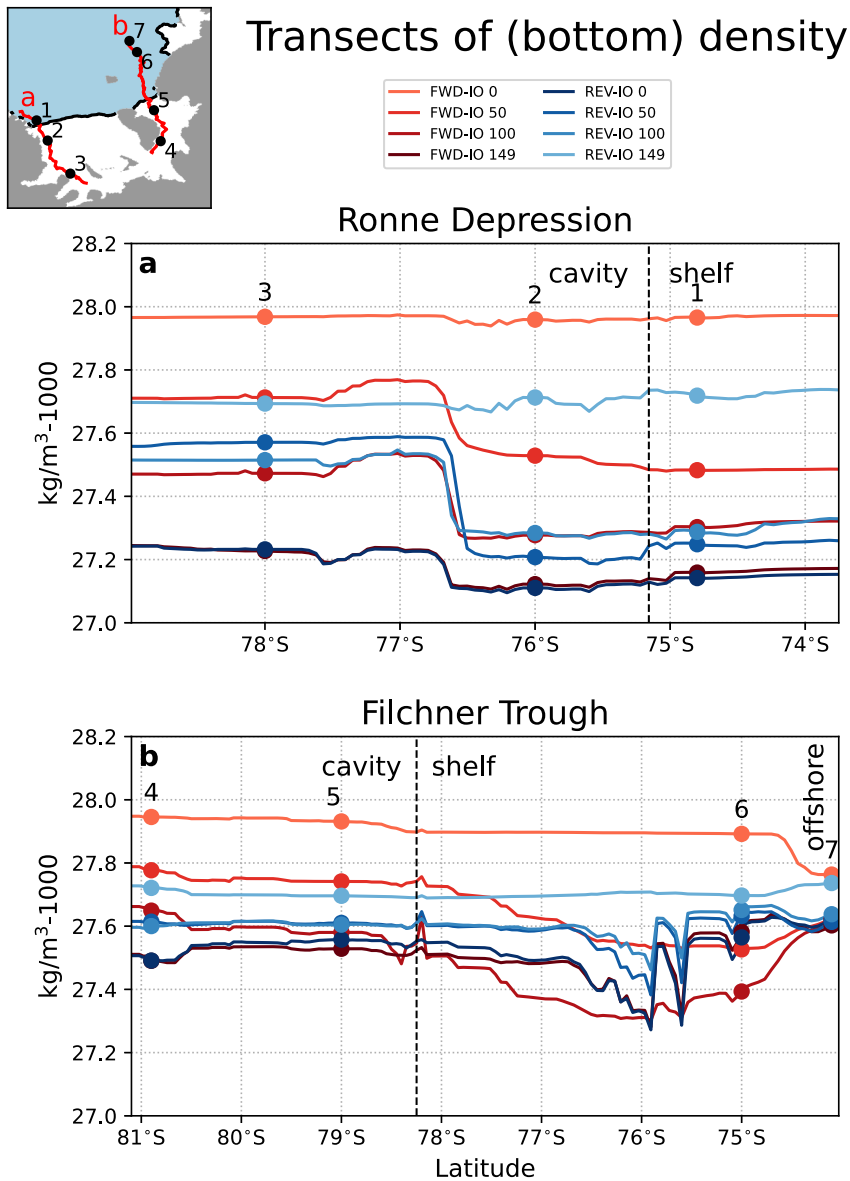

Figure 5. Transects of potential density at the bottom of the water column in the FRIS cavity and surrounding continental shelf. (a) Ronne Depression; (b) Filchner Trough. The transects are shown in the inset map and consist of the points with the deepest bathymetry at each model latitude, within the given regions. The transects are shown for every 50 years of the Fwd-IO (red) and Rev-IO-150 (blue) simulations. The points 1–7, are marked on both the density plots and the map, and correspond to the timeseries shown in Figure 6. The dashed vertical line in each panel shows the location of the ice front. South of this line is the ice shelf cavity, and north of this line is the continental shelf. A small amount of the continental slope and offshore region is shown in the northernmost extent of (b), where we extend values to be at a maximum depth of 600 m, which corresponds to the shallowest depth of Filchner trough.

also mixing through the entire water column occurs on the continental shelf, see Figure 7. While the temperatures in the cavity and on the continental shelf reverse to "cold" conditions, the salinity has not reached the initial values yet, with densities in the cavity still below their initial values.

To summarize, both transitions—the cold to warm as well as the warm to cold—show locally the abrupt shift in temperatures, when water masses at a location in the cavity change. In both cases, the change in water masses is related to a switch in density gradients which allows a change in circulation. Freshening and salinification of the cold surface waters, driven by the atmospheric forcing and sea-ice conditions on the continental shelf, as well as trends in the offshore WDW drive changes in water mass density. While in the forward simulation, the cavity flip

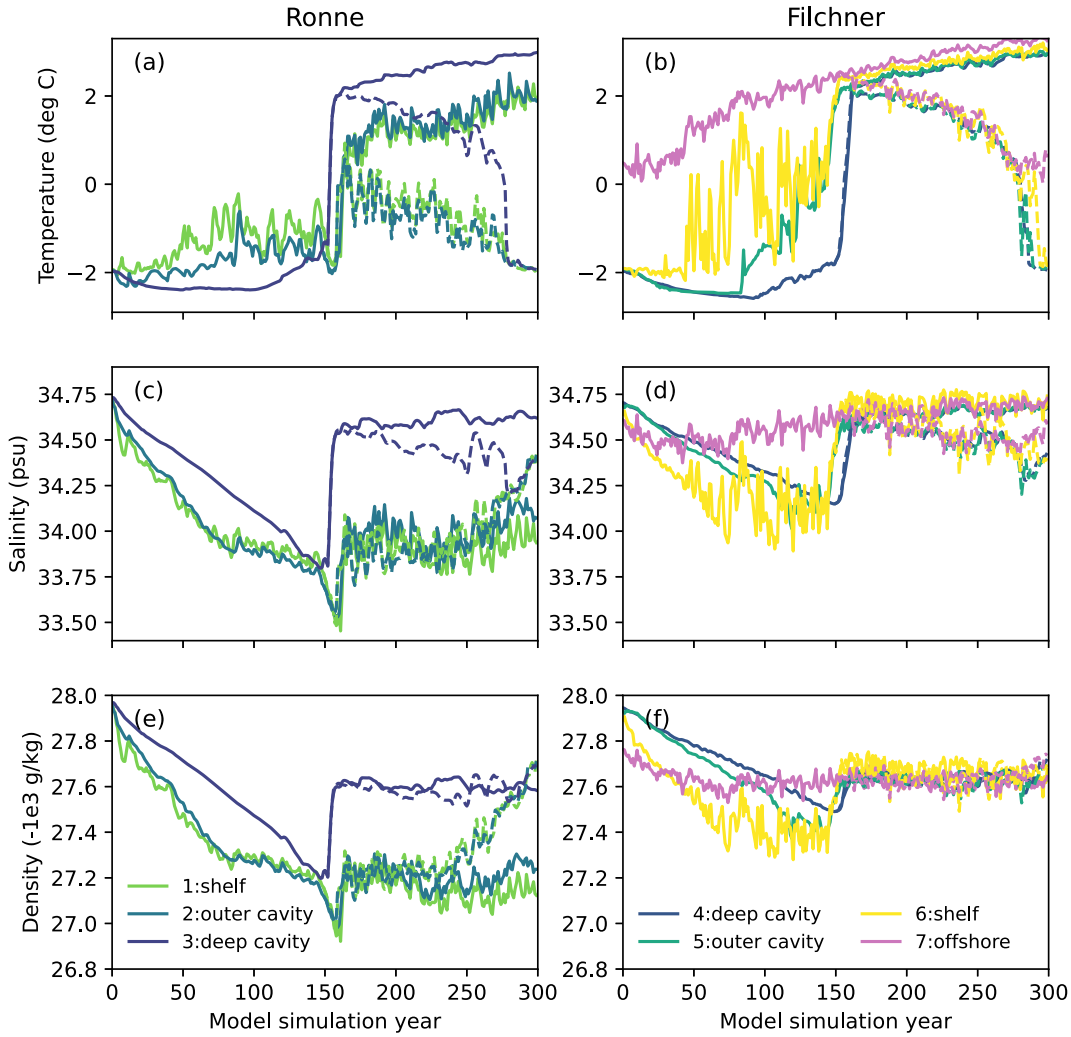

Figure 6. Evolution of (bottom) water mass properties in FRIS cavity and surrounding continental shelf. Evolution of (a, b) potential temperature, (c, d) practical salinity, and (e, f) potential density at the seven points located along the transects in Figure 5. Values are annual averages at the depth of the bathymetry, which are −613 m for point 1, −812 m for point 2, −1,287.5 m for point 3, −1513 m for point 4, −1363 m for point 5, −613 m for point 6, and at −600 m for offshore point 7. Solid lines show the forward (Fwd-IO) and dashed lines the reverse (Rev-IO-150) simulations.

is preceded by 75 years of warm water incursions, the major shift in sub-shelf melt rates occurs within less than two decades when the circulation through Filchner trough reverses. In the reverse run, melt rates decrease more gradually, as they initially mirror a trend in the offshore CDW and Filchner transport, and later on, they decrease gradually due to the time it takes to produce sufficiently salty and cold water at the surface that can mix through the water column and make its way through the cavity.

3.4. Ice-Ocean Feedbacks do Not Influence Reversibility

To quantify the centennial-scale impact of an evolving ice sheet on the ocean dynamics, we compare the results from our coupled simulations to ocean simulations with a fixed ice-shelf geometry. Aside from a consistently higher volume of basal mass loss, as noted in Section 3.2, we detect no discernible differences in the response to atmospheric changes between the static cavity simulations Fwd-O and Rev-O compared to the coupled Fwd-IO and Rev-IO simulations, see Figure 3a. In particular, the fixed cavity simulations exhibit a gradual cooling of the ocean temperature within the FRIS cavity, and sub-shelf melt rates reduce to present-day values at a comparable timescale. This indicates that, in our simulations, the regime shift and reversal of ocean conditions is entirely

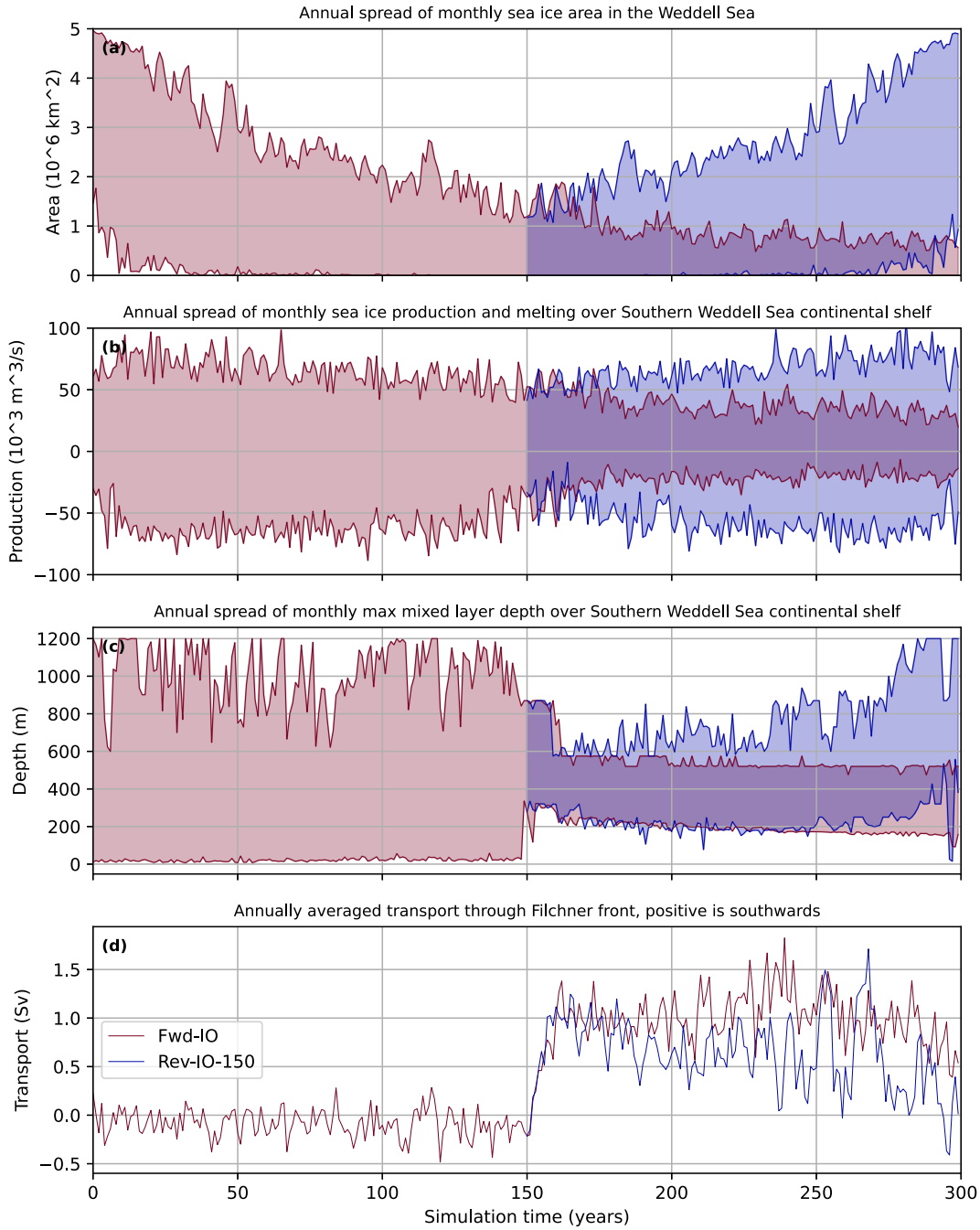

Figure 7. (a) Symmetry of 'cold-to-warm' and 'warm-to-cold' regime shifts. Panels (a–d) shows evolution of quantities in Fwd-IO and Rev-IO-150 runs to analyze symmetry and asymmetry of the regime shift and its reverse. Shown are yearly maximum and monthly minimum values of (a) sea ice area in the Weddell Sea, (b) sea ice production over the Southern Weddell Sea continental shelf, (c) maximum mixed layer depth over the Southern Weddell Sea continental shelf. Moreover, we show (d) annually averaged transport through the Filchner trough.

controlled by local atmospheric conditions and/or remote ocean forcing, and the evolving ice sheet geometry has little-to-no impact on the dominant changes in ocean dynamics.

We further test the relevance of the meltwater-feedback mechanism described by Hellmer et al. (2017). In our simulations, modeled rates of basal mass loss are in line with measurements and consistent with Hellmer et al. (2017), but there is considerable uncertainty in ocean model parameters that could lead to lower or

higher simulated melt rates once WDW floods the FRIS cavity. We adjust the amount of melt in fixed-cavity simulations by changing the value of the drag coefficient, C_d, in the basal melt parameterization (Holland & Jenkins, 1999; Losch, 2008). Halving (C_d = 0.00485, Fwd-O-low) or doubling (C_d = 0.0194, Fwd-O-high) its value leads to a reduction or amplification of the meltwater production by a factor of 0.7 (≈1,750 Gt/a) and 1.2 (≈3,000 Gt/a), respectively, see Figure 3 panel (c). We then repeated the Rev-O-150 in both cases (Rev-O-150-low and Rev-O-150-high in Figure 3), and found no discernible difference compared to the Rev-O-150 experiment. In particular, we recovered a cold cavity state over the same timescales irrespective of the almost 50% difference in freshwater input. The melt-overturning feedback discussed in Hellmer et al. (2017) does not seem to substantially alter the cavity dynamics in our simulations, in line with our simulations showing no indication of bi-stability, see Section 3.3. Further investigating the feedback might be key to understanding the existence of bi-stability.

3.5. Discussion

Our study highlights the difference in timescales of the ocean and ice sheet response. We found that ocean conditions recover at the end of the Rev-IO simulations. While the gradual reduction in melt during the 150 or 200 years of the reverse simulation means that the ice sheet experiences weaker ice shelf melting and buttressing loss than in the forward simulation, it still melts above the equilibrium levels from the control run and continues to retreat. Importantly, even if melt rates return to "cold" cavity conditions, the ice sheet has a longer response timescale and the full response to the melt perturbation will unfold over centennial to millennial timescales. In addition, the ice sheet could have entered a phase of MISI, in which reversing the melt rates is not sufficient to stop the internally driven, continued retreat (Hill et al., 2024).

Furthermore, we find a substantial difference in melt rates in the coupled versus standalone case, indicating that sub-shelf melt projections based on fixed-cavity modeling need to be used with caution. At the same time, our standalone simulations show a generally similar evolution of ocean temperature and salinity in comparison to the coupled simulations. If a sub-shelf melt parameterization for an ice sheet model, examples listed in Burgard et al. (2022), can be shown to respond well to changes in the geometry (which is as far as we know an open question at the moment), the ocean conditions from standalone models could be used to force an ice sheet model with ocean temperature and salinity instead of melt rates.

Our results on reversibility of the FRIS cavity can also be discussed in terms of hysteresis of the system. Hysteresis can mean "static hysteresis" which refers to the existence of multiple stable steady system states for a fixed control parameter and is equivalent to bi-stability. This definition has been applied for the Antarctic Ice Sheet (e.g., Garbe et al., 2020), and in previous studies of the Weddell Sea (Haid et al., 2023; Hazel & Stewart, 2020; Hellmer et al., 2017). While our results show no indication for static hysteresis, it shows "dynamic hysteresis", which is less strict and can also arise due to lags in the system in the absence of static hysteresis (An et al., 2021; Broner et al., 1997). In fact, while in our study the system is eventually reversible, the reversal takes more than a century, allowing for continued ocean-driven ice loss of 5 cm sea-level equivalent in our immediate ramp-down experiment and more than 10 cm sea-level equivalent in the delayed ramp-down experiment. This ice loss occurs during the reversal period, and further ice loss would occur afterward due to the long response time of ice sheets. Our experiments are designed to identify reversibility, and are not realistic, that is, they are based on a quadrupling of CO2 in 1850 and a simple mirrored ramp-down forcing, and hence time scales of ice loss might not be realistic. However, our experiments highlight that the longer the exposure to warm water masses lasts, as evidenced by the later reversal Rev-IO-200, the stronger the grounding line retreat, the ice loss, and sea-level contribution, with the potential of triggering irreversible, self-sustaining dynamics increasing.

We note that our results are based on one model, and more testing with different models would be required to assess structural uncertainty (De Rydt et al., 2024). Furthermore, to allow for high resolution, we conduct the experiments in a regional, Eddy-permitting ocean model with evolving cavities, which allows us to address the regime shift in detail. However, we cannot investigate the wider impact and feedbacks of future freshwater fluxes on the ocean in other Antarctic regions, and how they might impact reversibility. For example, the UKESM simulation that we use to force the ocean and atmospheric boundaries does include evolving surface runoff but not changes in sub-shelf melt or calving fluxes under warming, which can potentially drive surface freshening and sub-surface warming in circum-Antarctic simulations (Thomas et al., 2023), which could act to

cause an earlier "cold-to-warm" regime change of the cavity. We do not consider the fully coupled ice-sheet—ocean—atmosphere system in our domain, for example, we do not evolve the ice sheet surface mass balance, or retreat the calving front, or feed changing calving fluxes into the ocean model. While including surface runoff regionally would freshen the ocean, which could act to cause an earlier cold to warm change of the cavity, a retreated ice front would expose more ocean to the atmosphere and cool the shelf, potentially making recovery of the cavity easier. Calving fluxes could reduce when more ice shelf mass is lost through melting, but also increase once melting reduces ice shelf buttressing, which enhances ice flow, and thereby fracture and damage. Iceberg transport could be affected by the changes in wind stress/ocean transport, and it is hence open how warming might impact stratification and cooling fluxes from iceberg melting. It would be interesting future work to assess reversibility of the fully coupled system, which would be impacted by the viability of the ice shelf under such strong warming (Burgard et al., 2025). However, our experiments indicate that the interactions of cavity geometry changes through ocean-driven melting as well as the ocean circulation changes alone are not sufficient to make the system irreversible. Using a coupling time-step of 1 year, we average over the seasonal cycle, with the importance of seasonality in the Weddell Sea being something that requires to be assessed. Equally, we externally force atmospheric conditions, and hence lack ocean–atmosphere or sea ice–atmosphere feedbacks, with the atmospheric forcing data being low resolution which introduces particular uncertainties around the coastal winds and polynyas. Moreover, we use one forcing scenario, while alternative evolution of wind stress, temperature and surface freshwater fluxes in different cases could potentially allow for bi-stabilty (Hazel & Stewart, 2020; Haid et al., 2023; Hellmer et al., 2017). Furthermore, rewinding the CO2 concentrations in a global coupled model, instead of the atmosphere and ocean lateral boundaries, could allow for multi-stability to arise due to static hysteresis in other components of the climate system (Winkelmann et al., 2025).

4. Conclusions

Modeling the interactions of ice sheet and ocean in a coupled configuration of the Filchner-Ronne Ice Shelf, we find that while considering the coupled system is essential for melt rate projections, the regime shift and its reversibility is insensitive to the ice sheet response, and appears to be controlled by the local atmospheric conditions and/or remote ocean forcing. We find that the melt rate evolution of the "warm-to-cold" transition is asymmetric to the "cold-to-warm" transition and link this to trends in offshore WDW, strength of the Filchner inflow, and the time it takes to generate sufficiently dense and cold waters on the continental shelf to break down stratification and mix through the entire water column. Further work could establish how the meltwater feedback, sea ice conditions, and wind stress influence the existence of bi-stability. Furthermore, it would be of great interest to identify the climate forcing that commits the cold to warm regime shift to occur across models and scenarios, as well as the timescales between the commitment of a regime shift and the transition manifesting. In all our simulations, once initiated through warm water inflow, the ice sheet continuously loses mass and contributes to sea-level rise, with an open question being the reversibility of ice loss on longer time scales in the presence of ice-ocean feedbacks.

Conflict of Interest

The authors declare no conflicts of interest relevant to this study.

Availability Statement

The model setup and coupling scripts as well as the MITgcm and Úa versions used are available as "WSFRIS" from Naughten and De Rydt (2020). The timeseries generation code is available from Naughten and Jones (2023). Data and scripts to generate the figures are available from Reese et al. (2026).

Acknowledgments
This project has received funding from the European Union's Horizon 2020 research and innovation programme under Grant agreement no. 820575 (TiPACCs). RR was supported by the UKRI Natural Environment Research Council (Grant NE/Y001451/1, NE/Z503344/1). JDR was supported by a UKRI Future Leaders Fellowship (Grant. MR/W011816/1). KAN was supported by the NERC LTSM project TerraFIRMA (Future Impacts, Risks and Mitigation Actions in a changing Earth system). We would like to thank the members of TiPACCs Work Package 3 and Hartmut Hellmer from WP1 for fruitful discussions, and Irena Vaňková for helpful discussions on Filchner-Ronne Ice Shelf melting.

References

An, S.-I., Kim, H.-J., & Kim, S.-K. (2021). Rate-Dependent Hysteresis of the Atlantic Meridional Overturning Circulation System and Its Asymmetric Loop. *Geophysical Research Letters*, *48*, e2020GL090132. https://doi.org/10.1029/2020GL090132

Broner, F., Goldsztein, G. H., & Strogatz, S. H. (1997). Dynamical Hysteresis Without Static Hysteresis: Scaling Laws and Asymptotic Expansions. *SIAM Journal on Applied Mathematics*, *57*(4), 1163–1187. https://doi.org/10.1137/S0036139995290733

Burgard, C., Jourdain, N. C., Mosbeux, C., Caillet, J., Mathiot, P., & Kittel, C. (2025). Ocean warming threatens the viability of 60% of Antarctic ice shelves. *Nature*, *647*, 102–108. https://doi.org/10.1038/s41586-025-09657-w

Burgard, C., Jourdain, N. C., Reese, R., Jenkins, A., & Mathiot, P. (2022). An assessment of basal melt parameterisations for Antarctic ice shelves. *The Cryosphere*, *16*(12), 4931–4975. https://doi.org/10.5194/tc-16-4931-2022

De Rydt, J., & Gudmundsson, G. H. (2016). Coupled ice shelf-ocean modeling and complex grounding line retreat from a seabed ridge. *Journal of Geophysical Research: Earth Surface*, *121*, 865–880. https://doi.org/10.1002/2015JF003791

De Rydt, J., Jourdain, N. C., Nakayama, Y., van Caspel, M., Timmermann, R., Mathiot, P., et al. (2024). Experimental design for the Marine Ice Sheet–Ocean Model Intercomparison Project— Phase 2 (MISOMIP2). *Geoscientific Model Development*, *17*(18), 7105–7139. https://doi.org/10.5194/gmd-17-7105-2024

De Rydt, J., & Naughten, K. (2024). Geometric amplification and suppression of ice-shelf basal melt in West Antarctica. *The Cryosphere*, *18*(4), 1863–1888. https://doi.org/10.5194/tc-18-1863-2024

Garbe, J., Albrecht, T., Levermann, A., Donges, J. F., & Winkelmann, R. (2020). The hysteresis of the Antarctic Ice Sheet. *Nature*, *585*, 538–544. https://doi.org/10.1038/s41586-020-2727-5

Gudmundsson, G. H. (2013). Ice-shelf buttressing and the stability of marine ice sheets. *The Cryosphere*, *7*(2), 647–655. https://doi.org/10.5194/tc-7-647-2013

Haid, V., & Timmermann, R. (2013). Simulated heat flux and sea ice production at coastal polynyas in the southwestern Weddell Sea. *Journal of Geophysical Research: Oceans*, *118*, 2640–2652. https://doi.org/10.1002/jgrc.20133

Haid, V., Timmermann, R., Gürses, O., & Hellmer, H. H. (2023). On the drivers of regime shifts in the Antarctic marginal seas, exemplified by the Weddell Sea. *Ocean Science*, *19*(6), 1529–1544. https://doi.org/10.5194/os-19-1529-2023

Hazel, J. E., & Stewart, A. L. (2020). Bistability of the Filchner-Ronne Ice Shelf cavity circulation and basal melt. *Journal of Geophysical Research: Oceans*, *125*, e2019JC015848. https://doi.org/10.1029/2019jc015848

Hellmer, H. H., Kauker, F., Timmermann, R., Determann, J., & Rae, J. (2012). Twenty-first-century warming of a large Antarctic ice-shelf cavity by a redirected coastal current. *Nature*, *485*, 225–228. https://doi.org/10.1038/nature11064

Hellmer, H. H., Kauker, F., Timmermann, R., & Hattermann, T. (2017). The Fate of the Southern Weddell Sea Continental Shelf in a Warming Climate. *Journal of Climate*, *30*, 4337–4350. https://doi.org/10.1175/jcli-d-16-0420.1

Hill, E. A., Gudmundsson, G. H., & Chandler, D. M. (2024). Ocean warming as a trigger for irreversible retreat of the Antarctic ice sheet. *Nature Climate Change*, *14*, 1165–1171. https://doi.org/10.1038/s41558-024-02134-8

Holland, D. M., & Jenkins, A. (1999). Modeling Thermodynamic Ice–Ocean Interactions at the Base of an Ice Shelf. *Journal of Physical Oceanography*, *29*(8), 1787–1800. https://doi.org/10.1175/1520-0485(1999)029%3C1787:MTIOIA%3E2.0.CO;2

Holland, P., Bevan, S., & Luckman, A. (2023). Strong ocean melting feedback during the recent retreat of Thwaites Glacier. *Geophysical Research Letters*, *50*, e2023GL103088. https://doi.org/10.1029/2023GL103088

Janout, M. A., Hellmer, H. H., Hattermann, T., Huhn, O., Sültenfuss, J., Østerhus, S., et al. (2021). FRIS revisited in 2018: On the circulation and water masses at the Filchner and Ronne ice shelves in the southern Weddell Sea. *Journal of Geophysical Research: Oceans*, *126*, e2021JC017269. https://doi.org/10.1029/2021jc017269

Jourdain, N. C., Mathiot, P., Merino, N., Durand, G., Le Sommer, J., Spence, P., et al. (2017). Ocean circulation and sea-ice thinning induced by melting ice shelves in the Amundsen Sea. *Journal of Geophysical Research: Oceans*, *122*, 2550–2573. https://doi.org/10.1002/2016JC012509

Lenaerts, J. T. M., van den Broeke, M. R., van de Berg, W. J., van Meijgaard, E., & Kuipers Munneke, P. (2012). A new, high-resolution surface mass balance map of Antarctica (1979–2010) based on regional atmospheric climate modeling. *Geophysical Research Letters*, *39*, L04501. https://doi.org/10.1029/2011GL050713

Losch, M. (2008). Modeling ice shelf cavities in a z coordinate ocean general circulation model. *Journal of Geophysical Research*, *113*, C08043. https://doi.org/10.1029/2007JC004368

Marshall, J., Hill, C., Perelman, L., & Adcroft, A. (1997). Hydrostatic, quasi-hydrostatic, and nonhydrostatic ocean modeling. *Journal of Geophysical Research*, *102*(C3), 5733–5752. https://doi.org/10.1029/96JC02776

Mathiot, P., & Jourdain, N. C. (2023). Southern Ocean warming and Antarctic ice shelf melting in conditions plausible by late 23rd century in a high-end scenario. *Ocean Science*, *19*(6), 1595–1615. https://doi.org/10.5194/os-19-1595-2023

Met Office Hadley Centre. (2026). *WCRP CMIP6: Met Office Hadley Centre (MOHC) UKESM1-0-LL model output for the "abrupt-4xCO2" experiment*. Centre for Environmental Data Analysis. Retrieved from https://catalogue.ceda.ac.uk/uuid/3663b0d9d47443a786eca5ccdb32c18e

Morlighem, M., Rignot, E., Binder, T., Blankenship, D., Drews, R., Eagles, G., et al. (2020). Deep glacial troughs and stabilizing ridges unveiled beneath the margins of the Antarctic ice sheet. *Nature Geoscience*, *13*, 132–137. https://doi.org/10.1038/s41561-019-0510-8

Naughten, K., & De Rydt, J. (2020). *knaughten/UaMITgcm: UaMITgcm WSFRIS configuration (v1.0)*. Zenodo. https://doi.org/10.5281/zenodo.3876453

Naughten, K., & Jones, D. (2023). knaughten/mitgcm_python: mitgcm_python code for pre- and post-processing simulations of Naughten et al., 2023. (v1.0). *Zenodo*. https://doi.org/10.5281/zenodo.8263230

Naughten, K. A., De Rydt, J., Rosier, S. H., Jenkins, A., Holland, P. R., & Ridley, J. K. (2021). Two-timescale response of a large Antarctic ice shelf to climate change. *Nature Communications*, *12*(1), 1991. https://doi.org/10.1038/s41467-021-22259-0

Pritchard, H. D., Fretwell, P. T., Fremand, A. C., Bodart, J. A., Kirkham, J. D., Aitken, A., et al. (2025). Bedmap3 updated ice bed, surface and thickness gridded datasets for Antarctica. *Scientific Data*, *12*, 414. https://doi.org/10.1038/s41597-025-04672-y

Reese, R., De Rydt, J., & Naughten, K. (2026). Data and analysis scripts for "Ice-Sheet–Ocean Interactions and the Reversibility of a Regime Shift Beneath Filchner-Ronne Ice Shelf. *Zenodo*. https://doi.org/10.5281/zenodo.15748092

Reese, R., Garbe, J., Hill, E. A., Urruty, B., Naughten, K. A., Gagliardini, O., et al. (2023). The stability of present-day antarctic grounding lines—Part 2: Onset of irreversible retreat of Amundsen Sea glaciers under current climate on centennial timescales cannot be excluded. *The Cryosphere*, *17*(9), 3761–3783. https://doi.org/10.5194/tc-17-3761-2023

Sellar, A. A., Jones, C. G., Mulcahy, J. P., Tang, Y., Yool, A., Wiltshire, A., et al. (2019). UKESM1: Description and evaluation of the U.K. Earth System Model. *Journal of Advances in Modeling Earth Systems*, *11*, 4513–4558. https://doi.org/10.1029/2019MS001739

Strogatz, S. H. (2018). *Nonlinear Dynamics and Chaos: With Applications to Physics, Biology, Chemistry, and Engineering*. CRC Press.

Thomas, M., Ridley, J. K., Smith, I. J., Stevens, D. P., Holland, P. R., & Mackie, S. (2023). Future response of Antarctic continental shelf temperatures to ice shelf basal melting and calving. *Geophysical Research Letters*, *50*, e2022GL102101. https://doi.org/10.1029/2022GL102101

Timmermann, R., & Goeller, S. (2017). Response to Filchner–Ronne Ice Shelf cavity warming in a coupled ocean–ice sheet model—Part 1: The ocean perspective. *Ocean Science*, *13*(5), 765–776. https://doi.org/10.5194/os-13-765-2017

Vaňková, I., & Nicholls, K. W. (2022). Ocean variability beneath the Filchner-Ronne Ice Shelf inferred from basal melt rate time series. *Journal of Geophysical Research: Oceans*, *127*, e2022JC018879. https://doi.org/10.1029/2022JC018879

Vaughan, D. G., Barnes, D. K. A., Fretwell, P. T., & Bingham, R. G. (2011). Potential seaways across West Antarctica. *Geochemistry, Geophysics, Geosystems*, *12*, Q10004. https://doi.org/10.1029/2011GC003688

Winkelmann, R., Dennis, D. P., Donges, J. F., Loriani, S., Klose, A. K., Abrams, J. F., et al. (2025). The Tipping Points Modelling Intercomparison Project (TIPMIP): Assessing tipping point risks in the Earth system. *EGUsphere*, [preprint], 1–52. https://doi.org/10.5194/egusphere-2025-1899

Zeising, O., Steinhage, D., Nicholls, K. W., Corr, H. F. J., Stewart, C. L., & Humbert, A. (2022). Basal melt of the southern Filchner Ice Shelf, Antarctica. *The Cryosphere*, *16*(4), 1469–1482. https://doi.org/10.5194/tc-16-1469-2022